

Share Your Innovations through JACS Directory

Journal of Advanced Chemical Sciences

Visit Journal at https://www.jacsdirectory.com/jacs



Synthesis, Characterization and Visible Light Induced Photo-Degradation of Acid Orange II Dye in Aqueous Medium using a Novel Synthesized Al₂MoZnO₇ Nanocomposite

Shatarupa Basak¹, Salim Ali¹, Debasmita Das¹, Suranjan Sikdar², Mahendra Nath Roy^{1,*}

- ¹Department of Chemistry, University of North Bengal, Darjeeling 734013, West Bengal, India.
- ²Department of Chemistry, Govt. General Degree College at Kushmandi, Kushmandi, Dakshin Dinajpur 733121, West Bengal, India.

ARTICLEDETAILS

Article history: Received 26 June 2020 Accepted 18 July 2020 Available online 21 August 2020

Keywords: Zinc Oxide Fluorescence Photochemical Reaction Acid Orange II

ABSTRACT

The Al_2MoZnO_7 (AMZ) nanocomposite had been successfully synthesized via co-precipitation method followed by a low temperature calcinations treatment process. It had been found that such an Al_2MoZnO_7 nanocomposites exhibits higher photocatalytic activity and stability than pure ZnO towards the aqueous phase degradation of acid orange II dye under visible light (400 nm < λ). The presence of $Al^{3+}/Mo^{6+}/Zn^{2+}$ ions in Al_2MoZnO_7 and the formation of defects in the lattice are believed to play an essential role in influencing the photo-reactivity. The different types of active species scavengers are also play the photocatalytic process. The synthesized Al_2MoZnO_7 nanocomposites were characterized by UV-Vis spectroscopy, X-ray diffraction (XRD), SEM, TEM, EDAX and FTIR techniques. The average particle size and grain sizes of AMZ are around 6.5±0.3 nm and 50±5 nm measured from TEM and SEM respectively. The band gap energy AMZ and pure ZnO NPs was calculated from UV-Vis absorption and Tauc plot; and was found to be increased from 3.31 eV to 3.62 eV as Al and Mo co-doped in ZnO matrix. The optical absorption spectrum of ZnO NPs was blue shifted as co-doping of Al^{3+} and Al^{6+} ions in ZnO particles. In photoluminescence study showed that the effect of Al and Mo doped in ZnO NPs and the UV-emission peak was appeared around 323 nm. Photocatalytic study revealed that AMZ nanocomposite exhibited maximum degradation 82% for acid orange II dye under visible light irradiation within 50 minutes.

1. Introduction

Dyestuffs produced by Textile industries always constitute a largest number of organic compounds mainly phenolic derivatives which causes different environmental hazards and damage the human life. In the presence of a large number of aromatic groups in dye molecules and the stability of modern dyes, traditional and conventional techniques have been failure for the discoloration and degradation of dyes. Therefore, new methods are required for investigation which could conduct complete decomposition of dyes [1]. Most of the azo dyes are extensively used in textile, paper, leather, gasoline, additives, foodstuffs and cosmetics industry [2]. So it is very much essential to develop methods that can lead to destruction of such hazardous compounds. Removal of coloured contaminates from industrial effluents has been a major concerned for waste water treatment. There are so many physical methods [3], biological methods [4,5] and chemical methods [6] are most frequently employed for treatment of remove pollutants from dye industrial effluents. The presence of acid orange II dye, rhodamine B etc., an organic dye in discharged dye effluents is the most harmful for human beings [7-9]. For this purpose wide band gap containing metal oxide semiconductors are more attractive candidates for the removal of organic pollutants in water upon exposure to sun light radiation to degrade the harmful organic contaminants into harmless mineral acids. The most effective photocatalytic degradation of many dyes was carried out by using nanoparticles metal semiconductor oxides. Now-a-days, different kind of semiconductors has been studied as photocatalyst such as TiO2, ZnO, CdS, WO_3 , etc. Most of these semiconductor photocatalysts have band gap equivalent to or larger than 3.5 eV and promote photocatalysis upon irradiation with UV light. The limited amount of UV light in the Sun light (around 7%) stands as a big obstacle in the direct use of solar energy for photocatalytic decomposition of organic and inorganic contaminants [10,11]. Photocatalysis has been established as an efficient process for the mineralization of toxic organic compounds [12], hazardous inorganic materials [13] and microbial disinfection [14] in water as a result of the

[15]. Some of the commonly used metal oxide semiconductor photocatalysts are titanium dioxide (TiO2), zinc oxide (ZnO), tungsten oxide (WO₃), strontium titanate (SrTiO₃), and hematite (α-Fe₂O₃) [16-20]. Recently, it has been demonstrated that the semi-conducting materials mediated photocatalytic oxidation reactions of organic compounds are very successful, conventional alternative methods for the removal of organic pollutants from water [21-24]. Among the various photo catalytic semiconducting metal oxide, zinc oxide (ZnO) is considered to be a technologically prodigious material having a wide spectrum of applications such as that of a semiconductor (E_g = 3.37 eV), magnetic material, electroluminescent material, UV-absorber, piezoelectric sensor and actuator, nanostructure varistor, field emission displaying material, thermoelectric material, gas sensor, constituent of cosmetics etc., [25-27]. To overcome this ZnO is an excellent material with a large number of active sites and exhibits very high surface reactivity in visible light irradiation as compared to TiO_2 . High reaction and mineralization rates in ZnO photocatalysis have been reported due to the efficient generation of hydroxyl [28-30]. In ZnO, there is a multiplicity of levels, some deriving from residual impurities, some from oxygen deficiency, and others related to topographical irregularities [31,32]. Doping of non-metal and metal in ZnO nanoparticles can enhance the photo catalytic activity due to increase the surface defects, thereby affecting the optical and electronic transitions [33]. There are reports of the enhancement of optical absorption in ZnO by doping with transition metal ions such as Ag, Pb, Mn, and Co [34-39]. But no one can report the doping of Al and Mo codoped in ZnO. Sakthivel et al. have proved that ZnO can comparatively absorb more light than TiO2 in the region where the light absorption occurs due to band gap excitation [40,41]. The uses of ZnO as a photocatalyst for photodegradation of environmental pollutants has also been extensively studied, because of its nontoxic nature, low cost, and high photochemical reactivity. Bismuth oxide (Bi₂O₃) has been investigated extensively due to its optical and electrical properties such as refractive index, large energy band gap, dielectric permittivity as well as remarkable photoluminescence and photoconductivity. At the same time molybdenum has also crucial role for his catalytic activity. Therefore, the present work shows very much interest on nanocomposites due to different metal which has different properties and gives promising result. Doping of ZnO with non-metal and

formation of hydroxylradical (OH*), which acts as a strong oxidizing agent

^{*}Corresponding Author:mahendraroy2002@yahoo.co.in(Mahendra Nath Roy)

transition metals might shift the optical absorption of ZnO to the visible region. It was found that the presence of a small quantity of Al, Bi and Mo can effectively increase the photocatalytic efficiency of ZnO during the degradation of different organic dyes.

In this paper, the Al_2MoZnO_7 nanocomposites were prepared by coprecipitation method. The various influencing factors of Al_2MoZnO_7 nanocomposites photocatalytic degradation of acid orange II dye were investigated to enhance the photocatalytic efficiency. Furthermore, the kinetic equations of photocatalytic reaction and possible photocatalytic degradation mechanism were further evaluated and investigated.

2. Experimental Methods

2.1 Chemicals

All reagents aluminium nitrate nonahydrate [Al(NO₃)₃.9H₂O], ammonium heptamolybdate tetrahydrate [(NH₄)₆Mo₇O₂₄.4H₂O], zinc oxide (ZnO), ethylene glycol, and ethanol were provided from analytical grade, supplied from Merck Co. and conc.NH₄OH, hydrochloric acid (HCl) from AB Enterprises Mumbai, India. Acid orange II ($C_{16}H_{11}N_2NaO_4S$) was synthesized in our laboratory without purification.

Table 1 Physical properties and structure of acid orange II dye

	5 .
Name	Acid orange II dye
Molecular Formula	C ₁₆ H ₁₁ N ₂ NaO ₄ S
Molecular Weight	350.32
Appearance	Orange-Brown powder
PH	Amber to orange PH 7.4-8.6
λmax (nm)	484
Structure	Na+
	O O N N N
IUPAC name	Sodium 4-[(2E)-2-(2-oxonaphthalene-1-ylidene)hydrazinyl]benzenesulfonate

2.2 Synthesis of Al₂MoZnO₇ (AMZ) Nanocomposite

The nanocomposite of Al_2MoZnO_7 and pure ZnO nanoparticles were prepared by simple co-precipitation method. Initially, 2.370 g of $Al(NO_3)_3.9H_2O$ salt was immersed in deionized water under stirred condition till the Al-salt completely dissolved in it, then added small amount of dilute HCl to obtain clear solution. After that the solution was stirred for 30 minutes at 900 rpm followed by addition of 20 mL EtOH to this solution under same stirring condition. Again same way, 0.253 g of ZnO was dissolved in 20 mL distilled water in the presence of small amount of dilute HCl to prepare clear transparent Zn-salt solution and added the resulting solution to Al-salt solution drop by drop. Finally, we were added 0.539 g of $(NH_4)_6Mo_7O_{24}.4H_2O$ solution which was made up by dissolved it in 10 mL distilled water in the presence of small amount of dilute HCl, to the precursor solution and the resulting solution was stirred for an hour at room temperature.

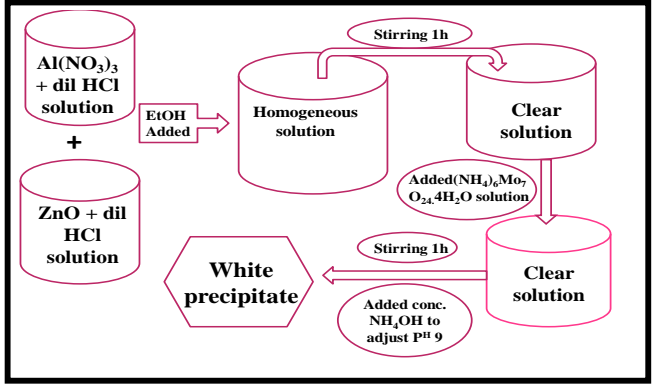


Fig. 1 Schematic flow chart diagram for synthesis of AMZ nanocomposite

After that concentrated NH $_4$ OH was added drop wise to the precursor solution under stirring condition and it was adjusted to pH 9.0, a white precipitated was immediately formed. The obtained precipitate was then filtered, washed with distilled water several times and ethanol. The precipitate was then dried in a vacuum oven at 150 °C and obtained the https://doi.org/10.30799/jacs.223.20060201

white powder, Al_2MoZnO_7 . The synthesis procedure is shown in Fig. 1. For comparison, same method was used to synthesize pure ZnO.

2.3 Characterization

The structure of the prepared nanocomposites were measured by X-ray diffractometer (XRD) at room temperature, using a XPERT-PRO PW3071 diffractometer with CuK α (λ =1.5418 Å) as target material using 40 kV accelerating voltage, 30 mA emission current. The initial absorbance of acid orange II (NO) dye was measured with the help of UV-vis spectrophotometer (Perkin Elmer Lambda 35). The average grain sizes of nanocomposites and atomic level dispersion were measured by scanning electron microscopy (SEM) and energy dispersive X-ray spectroscopy (EDX) (JEOL JMS-5800). FTIR spectra were recorded at room temperature using a Perkin-Elmer Paragon 1000 FT-IR spectrometer (JEOL JMS-5800). The fine structure of the prepared nanocomposites is analyzed by transmission electron microscopy (TEM) (TM-300, Philips). The DLS was measured by Zetasizer nano instrument. The PL spectra are recorded in JASCO FP 8500 spectroflurometer instrument equipped with 150 W Xe source between 200 and 700 nm for different excitation wavelength.

2.4 Photocatalytic Experiment

Acid orange II dye solution was made with an aqueous stock solution of $1000 \, \text{mg/L}$. The pH was adjusted with sodium hydroxide and hydrochloric acid solutions. The photocatalytic activity of the prepared nanocomposites, $Al_2 MoZnO_7$ is substantiated in the following procedure. The photocatalytic reaction was carried out under visible light irradiation. All the experiments were performed at room temperature. Reaction solutions were prepared by adding 0.05 g of AMZ photocatalyst nanopowder into 30 mL acid orange II dye. After photocatalytic process, the concentration of the solution was determined by absorption spectrometry using UV-vis spectrometer (PERKIN ELMER, LAMBDA 35) at its maximum absorption wavelength of 484 nm. The concentration reduction results and percent of photocatalytic degradation (%) was calculated with equation,

Removal efficiency % =
$$\left(\frac{c_0 - c}{c_0}\right) \times 100$$
 (1)

In this equation, C_0 is the initial concentration of dye solution and C is the final concentration of dye solution after the photocatalytic process. The experiments were done with different photocatalytic values for two synthesized samples and the results were presented as a reduction in dye concentration.

3. Results and Discussion

3.1 XRD Analysis

Fig. 2 illustrates the X-ray diffraction patterns for the nanostructure ZnO and co-doped ZnO nanocomposites. The high and sharp diffracted intensity of X-rays for nanostructure ZnO, it is clear that all the particles exhibit good crystalline nature. XRD pattern of Al and Mo co-doped ZnO nanocomposites samples were found almost same as that of pure ZnO nanoparticles. In pure ZnO nanoparticles, it was found that the different characteristic peaks were observed at an angle 2theta i.e. at 31.97, 34.62, 36.40, 47.67, 56.78, 63.05, 66.53, 68.15 and 69.22° which corresponds to miller indices (100), (002), (101), (102), (110), (103), (200), (112) and (201) respectively. All these peaks and miller indices are related to the standard hexagonal wurtzite crystal structure of pure ZnO NPs indexed and compared with ICPDS card No. 05-0664. It was found that the intense XRD peaks of AMZ were slightly shifting towards left from XRD peaks of pure ZnO nanoparticles due to some oxide defects in the crystals and well doping of Al3+ and Mo6+ ions in ZnO crystal lattice. It is clearly indicates that AMZ is a mixture of compositions of all the metal ions. Due to Al and Mo ions doping inside the periodic crystal lattice of ZnO, a small amount of strain is persuaded. This results in the swap of lattice which leads to change in the regularity of crystal. However, very careful inferences indicate that the peak position shifts towards the lower angle values as observed with doping of Al and Mo ions into ZnO matrix. Especially for the peaks located at i.e. 20 values are 25.82° and 29.35° indicates the shift towards lower value with doping, which can be attributed to the replacement of some Zn^{2+} ions by either Al^{3+} or Mo^{6+} ions. It is well reported in the literature that the lattice characteristics of the host materials get changed due to incorporation of dopant materials. This happens due to their variance in atomic radii of Al3+ and Mo6+ compared with Zn2+ ion radius. Although dopant ions may replace Zn ions, the basic structure of ZnO NPs is remain unaltered and they retain their original Wurtzite structure. The average crystallite size was calculated by using Debye-Scherer's formula;

$$D = \frac{0.9\lambda}{\beta \cos \theta} \tag{2}$$

where λ is the wavelength of the radiation (1.5406 Å), β is the full width at half maximum intensity and θ is the diffraction angle. From the calculated values, it is observed that the average crystalline size decreases with doping of Al and Mo ions (Table 2).

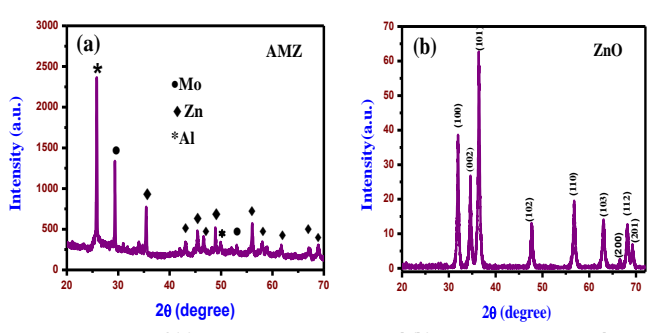


Fig. 2 XRD spectra of (a) AMZ nanocomposites and (b) pure ZnO nanoparticle

Table 2 Lattice parameters of pure ZnO and AMZ nanocomposites

Sample name	Lattice parameter			crystallite Size (nm)
	a(A ⁰)	c(A0)	c/a ratio	-
Pure ZnO NPs	3.24	5.20	1.605	24.13
AMZ	3.25	5.20	1.6	10.15

3.2 FTIR Spectra Analysis

Fig. 3 represents the FTIR spectra of the AMZ nanocomposites and pure ZnO nanoparticles which were obtained after calcinations at 500 °C in muffle furnace for 3 hours. It shows that nanocomposition of AMZ gives absorption peaks at 3469 cm⁻¹ corresponds to the strong O-H stretching mode of vibration is present on the surface due to moisture and there is also a weak and broad stretching vibration at 3199 cm⁻¹. The peak is appeared at 1618 cm⁻¹ due to the deformation vibration of HOH molecules. Below 600 cm⁻¹, a single strong peak around 437 cm⁻¹ was observed in Fig. 3(b). Fig. 3(a) exhibits three vibration bands in the range 500 to 925 cm⁻¹. These signals display stretching bands in the 500-925 cm⁻¹ range, associated with the vibrations of metal-oxygen, aluminium-oxygen and metal-oxygen-aluminium [42,43]. So the doped samples show the three peaks around 500-925 cm⁻¹ for the nanocomposites that is assigned to the formation of aluminium molybdenum zincates. The strong bands at 1405 cm-1 in the FTIR spectrum of AMZ is probably arising from stretching modes of vibration of C-H bonds. The absorption peaks at 595 cm⁻¹ corresponds to the stretching frequency of Mo=0...Mo bond present in AMZ nanocomposites.

The Fig. 3(b) shows the FTIR spectra of pure ZnO nanoparticles. The band at 3443 cm $^{\!-1}$ indicates the O-H stretching mode of vibration and the sharp peak at around 2360 cm $^{\!-1}$ suggesting the deformation vibration of H_2O molecules. The two weak bands at 1638 cm $^{\!-1}$ and 1385 cm $^{\!-1}$ with comparatively strong band at around 1483 cm $^{\!-1}$ assigned the characteristics bending vibrations of N-H, C-H bonds. The bands in the region at 1112 cm $^{\!-1}$ to 673 cm $^{\!-1}$ attributes the strong stretching vibrations of C-O and C-H bonds respectively. Finally the bands at 437 cm $^{\!-1}$ has assigned for Zn-O bond vibrations.

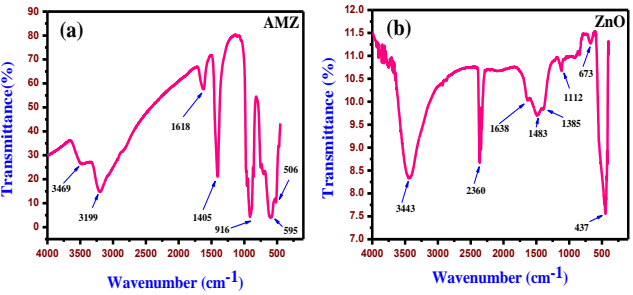


Fig. 3 The FTIR spectra of (a) AMZ nanocomposites and (b) pure ZnO nanoparticles

3.3 SEM Analysis

The study of morphology and structure were investigated using scanning electron microscopy and shown in Fig. 4 for AMZ and pure ZnO NPs. Pure ZnO showed that particle morphology as broken, irregular and flowerlike shape. A lot of ZnO nanoparticles with flowerlike morphology can be seen clearly from Fig. 4(b). According to the measurement, the particles sizes gave information about surface morphology of https://doi.org/10.30799/jacs.223.20060201

nanoparticles. Fig. 4(a) represents the SEM image of AMZ nanocomposites was also clearly seen that the surfaces are flakes in shape, some agglomeration was there and they are arranged in irregular manner and average grain sizes was found to be $\sim50\pm5$ nm.

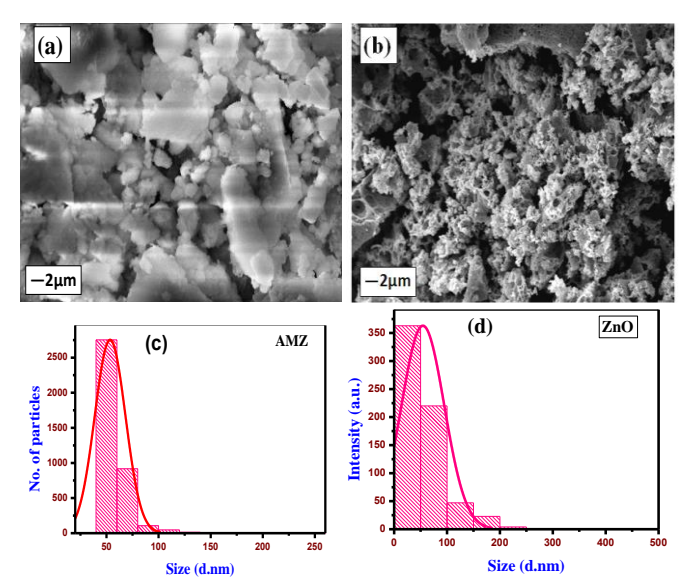


Fig. 4 SEM image of (a) AMZ nanocomposites, (b) ZnO and (c) the histogram for particle frequency and the grain size of the nanocomposites AMZ (d) pure ZnO; the average grain sizes were found to be 50 ± 5 nm and 20 ± 2 nm

3.4 Energy Dispersive X-Ray (EDX) Spectra Analysis

Elemental structure of AMZ and pure ZnO NPs were studied by use of energy dispersive X-ray (EDX) spectra analysis. In this study, investigation has done for the elemental composition of synthesized samples and for the confirmation of successful doping of Al $^{3+}$ Mo $^{6+}$ ions in ZnO matrix. The Fig. 5(a) represent the EDX signals and the percentage composition of AMZ sample were shown in table putting in the Fig. 5. The EDX spectrum of pure ZnO NPs and its percentage elemental analysis is also shown in Fig. 5(b). In this EDX signals, the peaks appearing in the areas 1-3, 8-10 and 18-20 keV are directly related to the characteristic of aluminum, molybdenum and zinc for synthesized AMZ nanocomposites. In addition, the peaks appearing in areas 0-2 and 8-10 keV related to Zn bonding energy (shown in Fig. 5(b)).

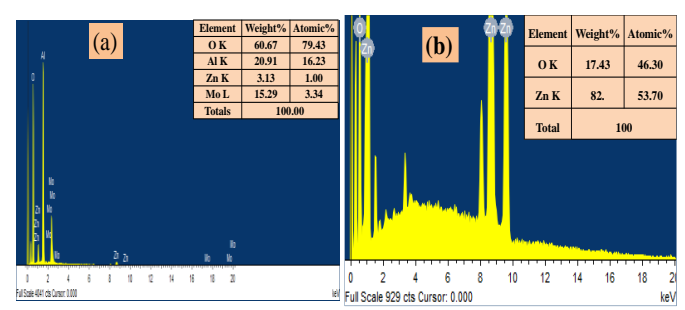


Fig. 5 EDAX spectrum of (a) AMZ nanocomposites and (b) pure ZnO NPs

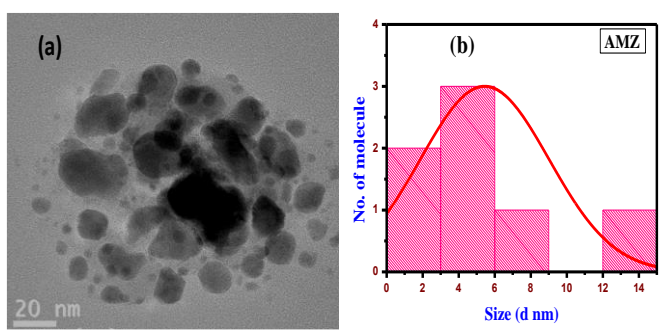


Fig. 6 (a) TEM image of AMZ nanocomposites and (b) the histogram for particle frequency and the particle size of the nanocomposites; the average diameter was $6.5\pm0.3~\text{nm}$

3.5 TEM Analysis

Fig. 6 exhibits the TEM image of AMZ nanocomposite particles. The particle size distributed between 1 nm and 15 nm. The average size of

nanocomposite particles was about $6.5\pm0.3\,$ nm, which is in agreement with the values obtained from Scherrer's formula. The particles are separated by well-defined boundaries, visible and uniformly distributed.

3.6 Determination of Optical Energy Band Gap Analysis

The optical band gap was determined from the analysis of the absorption spectrum as described by Tauc plot using the formula,

$$\alpha h \nu = \lambda_0 (h \nu - E_g)^n \tag{3}$$

In this equation, hv is the energy of incident photons and E_g is the value of the optical band gap corresponding to transitions indicated by the value of n. λ_0 is a constant which depends on the transition probability [44,45]. A best linear fit was found for n=0.5 which indicates an allowed direct transitions in the material. The extrapolation of the Tauc plot to the abscissa gives the value of the optical band gap shown in Fig. 7. The values of the AMZ and ZNPs were found to be 3.62 eV and 3.31eV respectively. The calculated optical band gap of pure ZnO NPs matches value given in literature [46-48]. For doping of Al $^{3+}$ and Mo $^{6+}$ ions in ZnO to form AMZ particles, the band gap was found to increase which indicates the blue shift ($\Delta E_g = 0.31$ eV). It is explained by quantum size effect, the smaller the crystallite size of the nanoparticles, the higher the band gap energy.

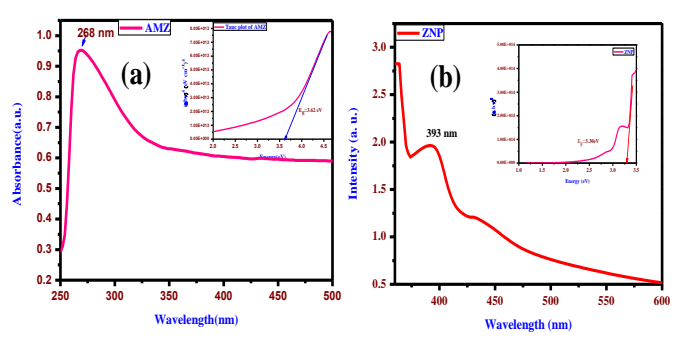
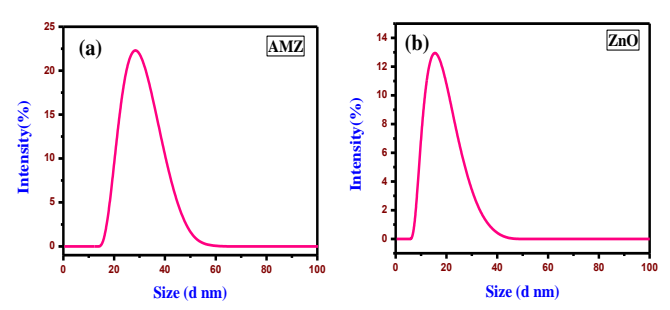


Fig. 7 (a) UV-vis absorption spectrum of AMZ and Tauc plot; (b) UV-vis absorption spectrum of pure ZnO nanoparticles and Tauc plot having energy band gap $3.62~\rm eV$ and $3.31~\rm eV$ respectively

3.7 Dynamic Light Scattering (DLS) Analysis

Particle size distribution was determined by dynamic light scattering analyzed based on measuring the time dependent fluctuation of scattering of light by nanoparticles undergoing Brownian movement [49,50]. Dynamic light scattering is widely used technique for the determination of particle size and surface charges of nanoparticles. In Fig. 8(a) and (b) show the particle size distribution of AMZ and ZnO NPs from which obtained the average particle size of AMZ and pure ZnO NPs and were found to be 28 nm and 16 nm respectively. The identical result is conformed to the XRD pattern [51-54]. Thus a good correlation is found among the XRD, SEM and DLS techniques which is experiment based similarity in size of nanoparticles, which ranges within 10 nm to 28 nm.



 $\boldsymbol{Fig.~8}$ DLS spectra of (a) AMZ and (b) pure ZnO NPs

3.8 Fluorescence Study

The room temperature photoluminescence (PL) spectra recorded for AMZ and ZnO nanoparticles are shown in Fig. 9. The PL spectra of AMZ nanocomposite exhibit the six emission peaks appeared at 293 nm, 305 nm, 322 nm, 418 nm, 539 nm and 586 nm and pure ZnO NPs also exhibits six peaks appeared at 367 nm, 377 nm, 402 nm, 422 nm, 475 nm and 664 nm. The strong emission peak observed at 322 nm and 539 nm respectively for AMZ particles and 402 nm and 664 nm for pure ZnO NPs which is assigned to the UV-visible emission. Generally the UV emission should be attributed to near band-edge emission of the wide band gap of AMZ and originated due to the slow exciton recombination between the photogenerated electrons in combination band and holes in the valence https://doi.org/10.30799/jacs.223.20060201

band. The near band edge emission at 402 nm was attributed to the free exciton recombination in ZnO reported [55,56]. The strong emission peak at 664 nm arises due to violet emission. In addition, a sharp blue emission peak observed at 475 nm corresponds to the single ionized oxygen vacancies in the ZnO and resulted from the recombination of a photon-generated hole with the single ionized charge state of the defects. As the Al³+ and Mo⁶+ doped is introduced into ZnO, the intensity of the emission peak is decreased when compared with that of pure ZnO which indicates that the number of vacancies decreased and UV emission peak position of AMZ experiences a blue shift from 664 nm to 539 nm. It was also found that the intensity of the emission peak is decreased with increase in concentration for both AMZ and pure ZnO NPs samples. This may be attributed by quenching effect which is caused by the formation of non-fluorescent dimers with increase in concentration.

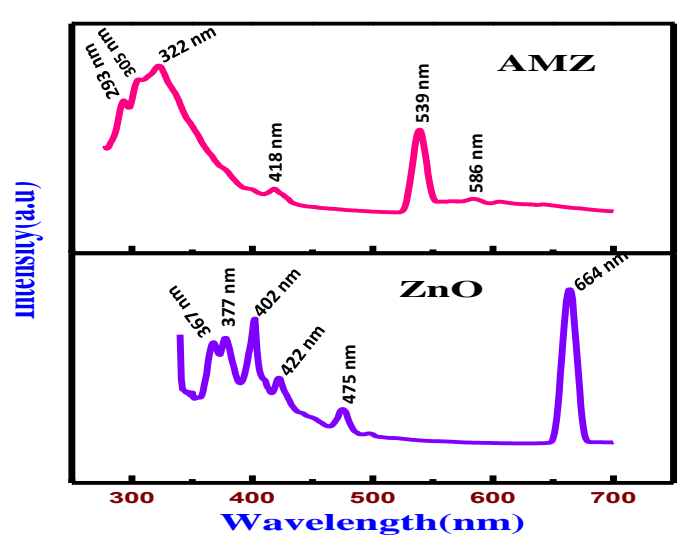


Fig. 9 Fluorescence spectra of AMZ nanocomposites and pure ZnO NPs

3.9 Photodegradation and Kinetics

The measurements of photoctatalytic activities were carried out for the AMZ nanocomposite and pure ZnO nanoparticles. The photocatalytic activities of AMZ catalyst was evaluated by measuring the degradation of NO in aqueous solution under visible light irradiation. In the present work, acid orange II was chosen as a model compound for photo degradation, since acid orange II dye is a good example of anionic azo dyes and non-biodegradable [57]. The photocatalytic activity of the samples can be evaluated quantitatively by comparing apparent speed of the reaction. Photo catalytic degradation generally follows Langmuir-Hinshelwood mechanism,

$$r = -\frac{dc}{dt} = \frac{kKC}{1+KC} \tag{4}$$

where r is the reaction rate, k is the rate constant and K is the absorption constant. If concentration is low, KC in the denominator is less than unity and can be ignored. So the rate Eq.(4) can be written as,

$$r = -\frac{dc}{dt} = kKC = k_{\rm app} C$$
 (5)

The integrated form of Eq.(5) leads to the following equation,

$$-ln(\frac{c}{CO}) = k_{app} C$$
 (6)

In this equation, C_0 , C and k_{app} are the initial concentration of dye, the dye concentration after photocatalytic degradation and apparent rate constant, respectively. By plotting of $-\ln(C/C_0)$ with time, k_{app} is obtained from the slope of the graphs (Table 3). The kinetic models of zero order, first order, second order and pseudo second order were used to investigate the photocatalytic degradation profiles. The results showed that the data were consistent with different kinetic models but the second order illustrated the best fitting with experimental data.

To study of reaction kinetics, 0.05~g of AMZ photocatalyst nanopowder AMZ and same amount of ZNP were taken in 30~mL acid orange II dye solutions into separate reaction vessels. Then a small volume of reactant liquid was siphoned out into a quartz cell and measures the UV-visible spectra in UV-Visible spectrophotometer at constant time interval of 10~minutes. It was found that the initial absorption peak of acid orange II dye appears at 484~nm with absorbance of 1.299~and their changes in presence of photocatalysts which are shown in Fig. 10(a)~and (b). After addition of the catalyst fades away the color of acid orange II dye slowly with the

progress of reaction and decreased gradually the characteristic peak of acid orange II dye at 484 nm with increasing the visible light exposure time. It was found that peak almost disappeared after 50 minutes of photocatalytic reaction for AMZ nanocomposites but surprisingly it was noticed that increase the absorption peak intensity in presence of ZnO nanparticles with no change of colour of acid orange II dye. This can be attribute that the Zn²+ ion may be for strong interaction with dye which is quite stable under the same reaction conditions. In Fig. 10(d) shows that after 50 minutes irradiation of acid orange II dye in presence of AMZ nanocomposite, the percentage of degradation is approximately $\sim\!82\%$.

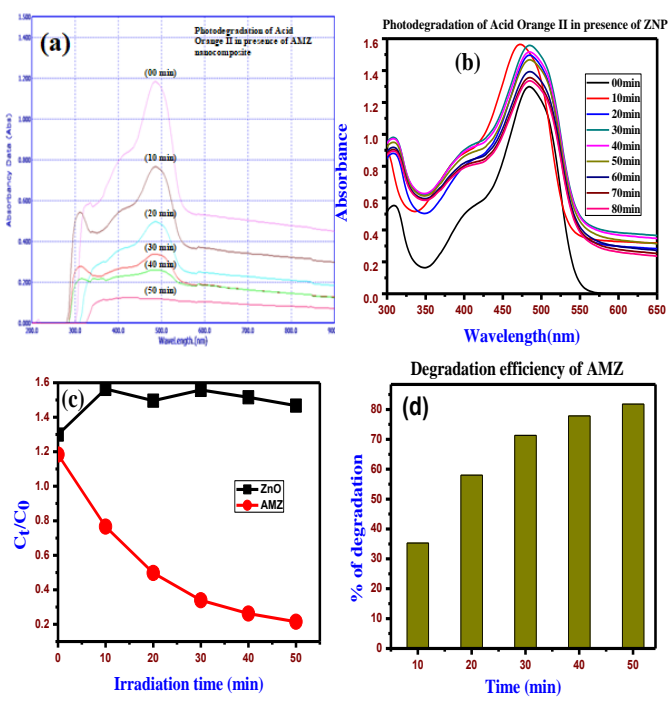


Fig. 10 Absorption spectra of photo-degradation by (a) AMZ and (b) ZnO; (c) kinetic photodegradation of acid orange II by different photocatalysts in 30 ppm dye solution with 0.05 g photocatalyst under visible light exposure 1 hour and (d) percentage of photodegradation by AMZ nanocomposite

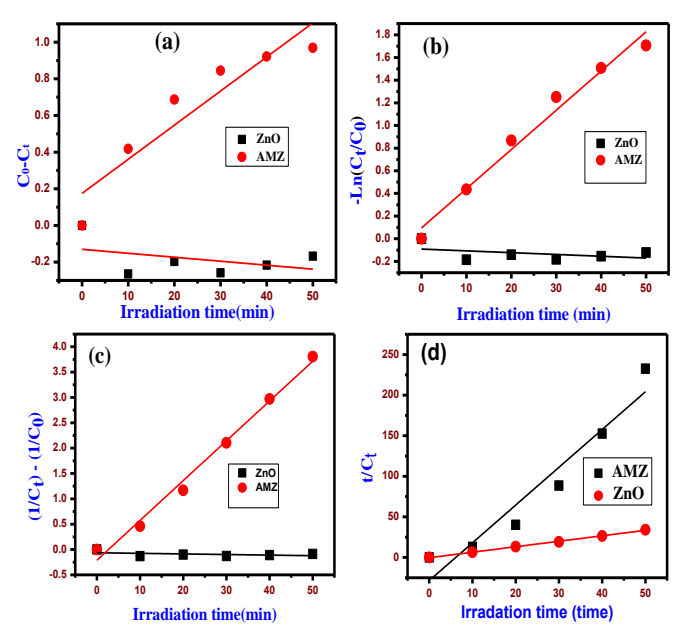


Fig. 11 Photocatalytic degradation linear kinetic models of (a) Zero-order, (b) first-order, (c) second-order and (d) pseudo-second-order of dye on different photocatalysts in 30 ppm dye solution with 0.05 g photocatalyst under visible light exposure 1 hour

Table 3 Linear kinetic models of the dye photocatalytic degradation

Model	Equation	Samples	k	R ²
Zero order	C_0 - C_t = kt	AMZ	0.01861	0.84708
First order	$Ln(C_t/C_0) = -kt$	AMZ	0.03466	0.97411
Second order	1/C t-1/C ₀	AMZ	0.07858	0.98787
Pseudo Second order	$t/C_t = t/C_0 - 1/kC_0^2$	AMZ	4.65684	0.91496

3.10 Mechanism of Photocatalytic Degradation

Mechanism of photodegradtion of acid orange II dye could be explained as: the Al and Mo incorporated ZnO is responsible for reducing photo-induced electron-hole charge recombination and prolongs the lifetime of photo-excited electrons. As shown in Fig. 12, after visible light irradiation of AMZ nanocomposites, the electrons are excited from valence band to conduction band and holes generated at VB of ZnO. Then the photo excited electrons are transferred from ZnO to AMZ because Al and Mo acts as an electron sink which ultimately generated 'OH radicals in the presence of oxygen molecule [58,59]. These 'OH radicals, superoxide radicals were responsible for the photodegradation of Acid orange II dye over AMZ nanocomposites. The following equations illustrate the photocatalytic reactions by the formation of carbon dioxide and water as products of the degradation as reported in different studies [60].

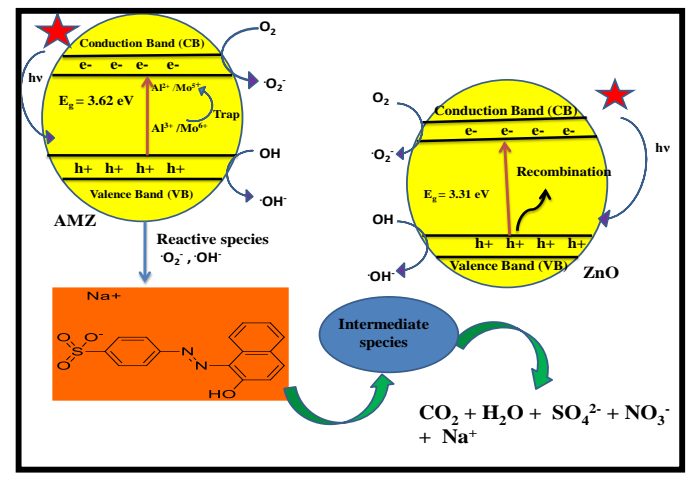
$$AMZ + hv \rightarrow e^{\cdot}_{(CB)} + h^{+}_{(VB)}$$
(7)

$$h^{+}_{(VB)} + 0H^{-} \rightarrow 0H^{+}$$
(8)

$$h^{+}_{(VB)} + H_{2}O \rightarrow 0H^{+}$$
(9)

$$O_{2} + e^{-} \rightarrow O_{2}^{-}$$
(10)

$$N_{0} + N_{0} + N_{0} + N_{0}^{-} + N_{0$$



 $\textbf{Fig. 12} \ Schematic \ diagrams \ showing \ the \ photo-catalytic \ mechanism \ of \ AMZ \ and \ pure \ ZnO \ nanoparticles$

4. Conclusion

In this research, highly stable dispersed Al₂MoZnO₇ (AMZ) nanocomposites were synthesized by the facile and simple coprecipitation process. The synthesized nanocomposites were characterized by UV-vis, XRD, EDX, SEM, TEM, DLS, photoluminescence and FTIR analyses and then used for photocatalytic degradation of an aqueous solution of acid orange II dye. The band gap investigations showed that AMZ increases the photocatalytic degradation of the resulting nanocomposite. The percentage of degradation efficiency by AMZ to acid orange II dye was found to be 82% during 50 min irradiation of visible light. Investigation of dye removal kinetic models showed the conformation of the second order model to the process of acid orange II dye degradation by synthetic nanocomposite. Our current work is expected to offer new insight into the AMZ nanocomposite as a photocatalyst under visible light irradiation.

Acknowledgements

The authors are thankful to the Department of Chemistry, Govt. General Degree College at Kushmandi, Dakshin Dinajpur, WB and Department of Chemistry, University of North Bengal, Darjeeling, WB for their assistant of instrumental support.

References

 L. Karimi, S. Zohoori, M.E. Yazdanshenas, Photocatalytic degradation of azo dyes in aqueous solutions under UV irradiation using nano-strontium titanate as the nanophotocatalyst, J. Saudi Chem. Soc. 18(5) (2014) 581–588.

- [2] K. Yamjala, M.S. Nainar, N.R. Ramisetti, Methods for the analysis of azo dyes employed in food industry, A review. Food. Chem. 192 (2016) 813–824.
- [3] S. Sharma, A. Bhattacharya, Drinking water contamination and treatment techniques, Appl. Water Sci. 7(3) (2016) 1043–1067.
- [4] D. Bhatia, N.R. Sharma, J. Singh, R.S. Kanwar, Biological methods for textile dye removal from wastewater: A review, Crit. Rev. Env. Sci. Tec. 47(19) (2017) 1836–1876.
- [5] K. Singh, S. Arora, Removal of synthetic textile dyes from wastewaters: A critical review on present treatment technologies, Crit. Rev. Env. Sci. Tec. 41(9) (2011) 807–878.
- [6] M.A. Barakat, New trends in removing heavy metals from industrial wastewater, Arab. J. Chem. 4(4) (2011) 361–377.
- [7] N.M. Julkapli, S. Bagheri, S.B.A. Hamid, Recent advances in heterogeneous photocatalytic decolorization of synthetic dyes, Sci. World J. 2014 (2014) 1–25.
- [8] A. Ahmad, S.H. Mohd-Setapar, C.S. Chuong, A. Khatoon, W.A. Wani, R. Kumar, M. Rafatullah, Recent advances in new generation dye removal technologies: novel search for approaches to reprocess wastewater, RSC Adv. 5(39) (2015) 30801–30818.
- [9] R.V. Kandisa, N. Saibaba, Dye removal by adsorption: A Review. J. Bioremed. Biodegr. 07(06) (2016) 371-374.
- [10] K. Maeda, Photocatalytic water splitting using semiconductor particles: History and recent developments, J. Photochem. Photobiol. C 12(4) (2011) 237–268.
- [11] C. Yu, L. Wei, J. Chen, Y. Xie, W. Zhou, Q. Fan, Enhancing the photocatalytic performance of commercial TiO₂ Crystals by coupling with trace narrow-bandgap Ag₂CO₃, Ind. Eng Chem. Res. 53(14) (2014) 5759–5766.
- [12] Y. Deng, R. Zhao, Advanced oxidation processes (AOPs) in wastewater treatment, Curr. Pollut. Rep. 1(3) (2015) 167–176.
- [13] R.V. Prihodko, N.M. Soboleva, Photocatalysis: Oxidative processes in water treatment, J. Chem. 2013 (2013) 1–8.
- [14] E.M. Cuerda-Correa, M.F. Alexandre-Franco, C. Fernández-González, Advanced oxidation processes for the removal of antibiotics from water: An overview, Water 12(1) (2019) 102-159.
- [15] V. Binas, D. Venieri, D. Kotzias, G. Kiriakidis, Modified TiO₂ based photocatalysts for improved air and health quality, J. Materiomics. 3(1) (2017) 3–16.
- [16] M. Mishra, D.M. Chun, α -Fe₂O₃ as a photocatalytic material: A review, Appl. Catal. A-Gen. 498 (2015) 126–141.
- [17] K. Siwińska-Stefańska, A. Kubiak, A. Piasecki, J. Goscianska, G. Nowaczyk, et al., TiO₂-ZnO binary oxide systems: Comprehensive characterization and tests of photocatalytic activity, Materials 11(5) (2018) 841-860.
- [18] S. Rehman, R. Ullah, A.M. Butt, N.D. Gohar, Strategies of making TiO₂ and ZnO visible light active, J. Hazard. Mater. 170(2-3) (2009) 560–569.
- [19] T.K. Townsend, N.D. Browning, F.E. Osterloh, Nanoscale strontium titanate photocatalysts for overall water splitting, ACS Nano. 6(8) (2012) 7420–7426.
- [20] A. Fakhri, S. Behrouz, Photocatalytic properties of tungsten trioxide (WO₃) nanoparticles for degradation of Lidocaine under visible and sunlight irradiation, Sol. Energy 112 (2015) 163–168.
- [21] S. Rasalingam, R. Peng, R.T. Koodali, Removal of hazardous pollutants from wastewaters: Applications of TiO₂-SiO₂ mixed oxide material, J. Nanomater. 2014 (2014) 1-42.
- [22] M.M. Mahlambi, C.J. Ngila, B.B. Mamba, Recent developments in environmental photocatalytic degradation of organic pollutants: The case of titanium dioxide nanoparticles—A review, J. Nanomater. 2015 (2015) 1–29.
- [23] W.S. Koe, J.W. Lee, W.C. Chong, Y.L. Pang, L.C. Sim, An overview of photocatalytic degradation: Photocatalysts, mechanisms, and development of photocatalytic membrane, Environ. Sci. Pollut. Res. 27 (2020) 2522–2565.
- [24] A. Ajmal, I. Majeed, R.N. Malik, H. Idriss, M.A. Nadeem, Principles and mechanisms of photocatalytic dye degradation on TiO₂ based photocatalysts: A comparative overview, RSC Adv. 4(70) (2014) 37003–37026.
- [25] S.C. Rai, K. Wang, Y. Ding, J.K. Marmon, M. Bhatt, et al., Piezo-phototronic effect enhanced UV/visible photodetector based on fully wide band gap type-II ZnO/ZnS core/shell nanowire arra, ACS Nano. 9(6) (2015) 6419–6427.
- [26] S.J. Kim, D.W. Park, Preparation of ZnO nanopowders by thermal plasma and characterization of photo-catalytic property, Appl. Surf. Sci. 255(10) (2009) 5363-5367.
- [27] Z.L. Wang, Energy harvesting for self-powered nanosystems, Nano Res. 1(1) (2008) 1–8.
- [28] P. Velusamy, G. Lakshmi, Enhanced photocatalytic performance of (ZnO/CeO₂)β-CD system for the effective decolorization of Rhodamine B under UV light irradiation, Appl. Water Sci. 7(7) (2017) 4025–4036.
- [29] P. Raizada, A. Sudhaik, P. Singh, Photocatalytic water decontamination using graphene and ZnO coupled photocatalysts: A review, Mater. Sci. Eng. Tec. 2(3) (2019) 509-525.
- [30] M. Pawar, S. Topcu Sendoğdular, P. Gouma, A brief overview of TiO₂ photocatalyst for organic dye remediation: Case study of reaction mechanisms involved in Ce-TiO₂ photocatalysts system, J. Nanomater. 2018 (2018) 1–13.
- [31] S. Baruah, S.S. Sinha, B. Ghosh, S.K. Pal, A.K. Raychaudhuri, J. Dutta, Photoreactivity of ZnO nanoparticles in visible light: Effect of surface states on electron transfer reaction, J. Appl. Phys. 105(7) (2009) 074308:1-6.
- [32] S.C. Sharma, ZnO nano-flowers from Carica papaya milk: Degradation of alizarin red-S dye and antibacterial activity against Pseudomonas aeruginosa and Staphylococcus aureus, Optik. 127(16) (2016) 6498–6512.

- [33] R. Saleh, N.F. Djaja, Transition-metal-doped ZnO nanoparticles: Synthesis, characterization and photocatalytic activity under UV light, Spectrochim. Acta A Mol. Biomol. Spectrosc. 130 (2014) 581–590.
- [34] R. Marschall, L. Wang, Non-metal doping of transition metal oxides for visible-light photocatalysis, Catal. Today 225 (2014) 111-135.
- [35] K. Pradeev Raj, K. Sadaiyandi, A. Kennedy, S. Sagadevan, Z.Z. Chowdhury, et al., Influence of Mg doping on ZnO nanoparticles for enhanced photocatalytic evaluation and antibacterial analysis, Nanoscale Res. Lett. 13(1) (2018) 229-242.
- [36] M.E. Ashebir, G.M. Tesfamariam, G.Y. Nigussie, T.W. Gebreab, Structural, optical, and photocatalytic activities of Ag-Doped and Mn-doped ZnO nanoparticles, J. Nanomater. 2018 (2018) 1–9.
- [37] P. Singh, R. Kumar, R.K. Singh, Progress on transition metal-doped ZnO nanoparticles and its application, Ind. Eng. Chem. Res. 58(37) (2019) 17130-17163
- [38] D. Sharma, R. Jha, Transition metal (Co, Mn) co-doped ZnO nanoparticles: Effect on structural and optical properties, J. Alloys Compd. 698 (2017) 532–538.
- [39] Y. Lu, Y. Lin, T. Xie, S. Shi, H. Fan, D. Wang, Enhancement of visible-light-driven photoresponse of Mn/ZnO system: photogenerated charge transfer properties and photocatalytic activity, Nanoscale 4(20) (2012) 6393-6400.
- [40] S.A. Ansari, M.M. Khan, M.O. Ansari, M.H. Cho, Nitrogen-doped titanium dioxide (N-doped TiO₂) for visible light photocatalysis, New J. Chem. 40(4) (2016) 3000–3009.
- [41] M. Rostami, Construction of La-doped TiO₂@La-doped ZnO-B-doped reduced graphene oxide ternary nanocomposites for improved visible light photocatalytic activity, RSC Adv. 7(69) (2017) 43424–43431.
- [42] M.U. Shahid, K.M. Deen, A. Ahmad, M.A. Akram, M. Aslam, W. Akhtar, Formation of Al-doped ZnO thin films on glass by sol-gel process and characterization, Appl. Nanosci. 6(2) (2015) 235–241.
- [43] V. Saxena, P. Chandra, L.M. Pandey, Design and characterization of novel Aldoped ZnO nanoassembly as an effective nanoantibiotic, Appl. Nanosci. 8 (2018) 1925–1941.
- [44] N. Ghobadi, Band gap determination using absorption spectrum fitting procedure, Int. Nano Lett. 3 (2013) 1-4.
- [45] P. Makuła, M. Paci, W. Macyk, How To correctly determine the band gap energy of modified semiconductor photocatalysts based on UV-Vis spectra, J. Phys. Chem. Lett. 9(23) (2018) 6814–6817.
- [46] A. Sáenz-Trevizo, P. Amézaga-Madrid, P. Pizá-Ruiz, W. Antúnez-Flores, M. Miki-Yoshida, Optical band gap estimation of ZnO nanorods, Mater. Res. 19 (2016) 33-38
- [47] M. Sajjad, I. Ullah, M.I. Khan, J. Khan, M.Y. Khan, M.T. Qureshi, Structural and optical properties of pure and copper doped zinc oxide nanoparticles, Results Phys. 9 (2018) 1301–1309.
- [48] K. Davis, R. Yarbrough, M. Froeschle, J. White, H. Rathnayake, Band gap engineered zinc oxide nanostructures via a sol-gel synthesis of solvent driven shape-controlled crystal growth, RSC Adv. 9(26) (2019) 14638-14648.
- [49] S. Krishnaswamy, P. Panigrahi, G.S. Nagarajan, Tailoring the optical properties of ZnO thin film by citrus limon doped polypyrrole, J. Mater. Sci. Mater. Electron. 31 (2020) 8502–8513.
- [50] P.A. Hassan, S. Rana, G. Verma, Making sense of Brownian motion: Colloid characterization by dynamic light scattering. Langmuir 31(1) (2014) 3–12.
- [51] J. Stetefeld, S.A. McKenna, T.R. Patel, Dynamic light scattering: a practical guide and applications in biomedical sciences, Biophys. Rev. 8(4) (2016) 409–427.
- [52] X. Fuku, A. Diallo, M. Maaza, Nanoscaled electrocatalytic optically modulated ZnO nanoparticles through green process of *Punica granatum* L. and their antibacterial activities, Int. J. Electrochem. 2016 (2016) 1–10.
- [53] A. Narayana, S.A. Bhat, A. Fathima, S.V. Lokesh, S.G. Surya, C.V. Yelamaggad, Green and low-cost synthesis of zinc oxide nanoparticles and their application in transistor-based carbon monoxide sensing, RSC Adv. 10(23) (2020) 13532– 13542.
- [54] W. Muhammad, N. Ullah, M. Haroon, B.H. Abbasi, Optical, morphological and biological analysis of zinc oxide nanoparticles (ZnO NPs) using *Papaver* somniferum L, RSC Adv. 9(51) (2019) 29541–29548.
- [55] Y. Liang, S. Wicker, X. Wang, E. Erichsen, F. Fu, Organozinc precursor-derived crystalline ZnO nanoparticles: Synthesis, characterization and their spectroscopic properties, Nanomater. 8(1) (2018) 22-45.
- [56] A. Artesani, S. Bellei, V. Capogrosso, A. Cesaratto, S. Mosca, et al., Photoluminescence properties of zinc white: an insight into its emission mechanisms through the study of historical artist materials, Appl. Phys. A. 122(12) (2016) 1053-1064.
- [57] A. Singh, K. Senapati, B. Satpati, P.K. Sahoo, Suppression of near band edge emission in specially engineered ZnO twin nanorods, Phys. Chem. Chem. Phys. 19(21) (2017) 14012–14019.
- [58] K. Tanaka, K. Padermpole, T. Hisanaga, Photocatalytic degradation of commercial azo dyes, Water Res. 34(1) (2000) 327–333.
- [59] K. Azad, P. Gajanan, Photodegradation of methyl orange in aqueous solution by the visible light active Co:La:TiO₂ nanocomposite, Chem. Sci. J. 08(03) (2017) 1.0
- [60] Y.H. Chiu, T.F. M. Chang, C.Y. Chen, M. Sone, Y.J. Hsu, Mechanistic insights into photodegradation of organic dyes using heterostructure photocatalysts, Catalysts. 9(5) (2019) 430-462.